MSEAS-ParEq for Coupled Ocean-Acoustic Modeling around the Globe

Wael H. Ali[a,b], Aaron Charous[a,b], Chris Mirabito[a,b], Patrick J. Haley, Jr.[a,b], Pierre F. J. Lermusiaux[a,b,†]
[a] *Department of Mechanical Engineering, Massachusetts Institute of Technology, Cambridge, MA*
[b] *Center for Computational Science and Engineering, Massachusetts Institute of Technology, Cambridge, MA*
[†]Corresponding Author: pierrel@mit.edu

***Abstract*—The multi-scale dynamics of oceanic processes and the complex propagation of acoustic waves are fundamental challenges in marine sciences and operations. Recent computing advances enable such multiresolution ocean and acoustic modeling, but a fully integrated system for sustained coupled predictions and Bayesian data assimilation remains needed. In this study, we integrate the MSEAS Primitive Equation (PE) ocean modeling system and the MSEAS acoustic Parabolic Equation (ParEq) solver, enabling real-time coupled ocean and acoustic predictions. Realistic applications in Massachusetts Bay, the Norwegian Sea, the western Mediterranean Sea, and the New York Bight are used to demonstrate capabilities and validate predictions in diverse shallow and deep-water environments. Results provide the foundation for an end-to-end system for coupled ocean-acoustic probabilistic modeling, Bayesian inversion, and learning.**

***Index Terms*—ocean modeling, acoustic modeling, coupled system, end-to-end predictions, primitive equations, parabolic equation, data assimilation**

I. Introduction

Understanding and predicting the intricate dynamics of oceanic processes and the complex propagation of acoustic waves are fundamental challenges in marine sciences. The ocean's changing physical properties, such as temperature, salinity, and currents, introduce significant complexities that directly impact sound waves [1–3]. Furthermore, limited data availability and sparse monitoring networks pose substantial hurdles for accurate modeling and forecasting [4, 5]. Despite these challenges, the importance of coupled ocean-acoustic modeling cannot be overstated. On one hand, high-resolution ocean models, equipped with advanced data assimilation, can provide detailed and dynamic representations of the sound speed fields and acoustically-relevant features such as internal tides, fronts, eddies, jets, and currents [6–10]. On the other hand, underwater acoustic propagation is influenced by oceanic scales significantly smaller than those captured by the majority of regional models [6, 9, 11]. Therefore, by integrating acoustic data with traditional ocean measurements, important small-scale corrections can be made enhancing the resolution of the temperature, salinity, and current fields predicted by regional ocean models [12, & references therein]. For instance, ocean acoustic tomography provides average temperature profiles over range using acoustic travel time measurements [13–15]. More generally, utilizing all of the information contained in the limited data to estimate and predict the ocean environment and the acoustic fields jointly requires an integrated system for coupled ocean-acoustic modeling and multivariate Bayesian estimation [7, 16–19].

Over the past several decades, advances in computer technology and in ocean observation technologies have dramatically improved our ability to predict the ocean environment using high-resolution numerical models and data assimilation [20]. Likewise, computing progress enabled new underwater acoustic modeling and led to advances in ray theory, normal modes, wavenumber integration, and parabolic equation propagation models [3, 4, 21]. Coupled ocean-acoustic models have also followed suit, and systems that forecast the ocean state and acoustic propagation have been recently developed. One of the early works on integrated ocean-acoustic modeling in 3D includes linking the Harvard Open Ocean Model with the acoustic parabolic equation models FOR3D and IFD [11, 22–26]. More recently, ocean-acoustic models were developed as physical-acoustic-sonar end-to-end systems to evaluate tactical system performances [5, 8, 16, 27]. The deployment of such ocean-acoustic models in real-time experiments and multiscale ocean scenarios prompted research into quantifying uncertainties in ocean model fields and parametrizations, and explaining their effects on acoustic propagation [6, 9, 19, 28–30]. Bayesian-based systems were then initiated using the Error Subspace Statistical Estimation (ESSE) [7, 31]. Related work includes variational data assimilation systems based on the adjoint of the acoustic parabolic equation [32, 33] or using neural-network-based acoustic observation operators [18].

The present work builds and evaluates a multi-resolution coupled ocean-acoustic modeling system for realistic deterministic ocean and acoustic predictions in various shallow and deep water environments. It is a first step towards an end-to-end system for coupled ocean-acoustic stochastic modeling and Bayesian inversion that would combine acoustic uncertainty quantification using the Dynamically Orthogonal Parabolic Equations [34–37] with multidisciplinary Bayesian inversion using Gaussian Mixture Models [38]. Specifically, we integrate our MIT Multidisciplinary Simulation, Estimation, and Assimilation Systems (MSEAS) Primitive Equation (PE) ocean modeling system [39, 40] and the MSEAS acoustic parabolic equation (ParEq) model [34, 35]. The MSEAS-PE has been used for real-time data-assimilative forecasting in many regions around the world's oceans. The MSEAS-ParEq solves the range-dependent narrow-angle [41] and wide-angle ParEqs [3]. Their full integration provides bottom topography, sediment characteristics, sound speed, and density fields, along with acoustic pressure and transmission loss (TL) fields.

In what follows, in section II, we describe the MSEAS-PE ocean and MSEAS-ParEq acoustic solvers, and their integration. In section III, we apply and validate the coupled ocean-acoustic system in real-time sea exercises and multiresolution modeling scenarios. Finally, we conclude in section IV.

979-8-218-14218-6 ©2023 MTS

II. Methodology

A. MSEAS-PE Ocean Modeling System

The MIT MSEAS-PE ocean modeling system [39, 40] has been used for fundamental research and for realistic simulations in varied regions of the World Ocean [42–50]. The MSEAS-PE is based on a nonlinear free-surface hydrostatic primitive-equation model, using second-order structured finite volumes and configured with generalized-level vertical coordinates and implicit two-way nesting. Its strengths include its ability to simulate (sub)-mesoscale processes over nested domains with complex geometries and varied interactions, using an implicit two-way nesting/tiling. The specific subsystems we employ include initialization schemes [40], nested tidal prediction and inversion [51], fast-marching coastal objective analysis [52], subgrid-scale models [31, 53], and advanced data assimilation [54, 55]. The MSEAS-PE applications include monitoring [56], ecosystem prediction and environmental management [57, 58], and oceanographic-acoustic hindcasts and ocean-acoustic data assimilation [see 5, 8, 59–62].

B. MSEAS-ParEq Acoustic Solvers

The MSEAS-ParEq system solves the acoustic narrow-angle parabolic equation (NAPE) [41] and several versions of the Padé wide-angle parabolic equation (WAPE) [3, 63, 64]. It uses second-order spatial finite volume (FV) schemes for the transverse space operators and high-order range marching schemes (e.g., second-order backward difference, Crank-Nicholson, and high-order Runge-Kutta). It supports initial range conditions given by analytical starters (Gaussian, Greene) [3] and self-starter initialization [65, 66]. To enable the end-to-end modeling discussed in the introduction, a highly efficient acoustic modeling framework is needed. The solvers employ efficient matrix-free, operation, and dimension splitting techniques allowing for propagation in large domains and have been validated on several benchmark cases [34, 35].

C. Integrated MSEAS-PE and MSEAS-ParEq

The MSEAS-ParEq was tightly coupled with the MSEAS-PE. This software coupling enables simulating acoustic propagation in realistic ocean environments, as demonstrated in section III. The bottom topography, sound speed, and density fields from the MSEAS-PE ocean simulations are provided as inputs to the MSEAS-ParEq solver. Specific software was written for such coupling. As the MSEAS-PE simulation progresses, relevant environmental fields are provided to the MSEAS-ParEq, allowing parallel acoustic computing in multiple sections, simultaneously with ocean computing.

III. Realistic Applications and Validations

We apply our integrated systems in four regions and time periods: (a) Massachusetts Bay and surrounding waters in August/September 2019; (b) the Norwegian Sea in January 2017; (c) the western Mediterranean Sea in November 2016; and (d) the New York Bight in June/July 2009. The modeling domains are shown in figure 1. Our MSEAS-ParEq acoustic system is flexible. It has also been used with the HYbrid Coordination Ocean Model (HYCOM), for hindcasting in the North Atlantic Ocean. We refer to [67] for further details.

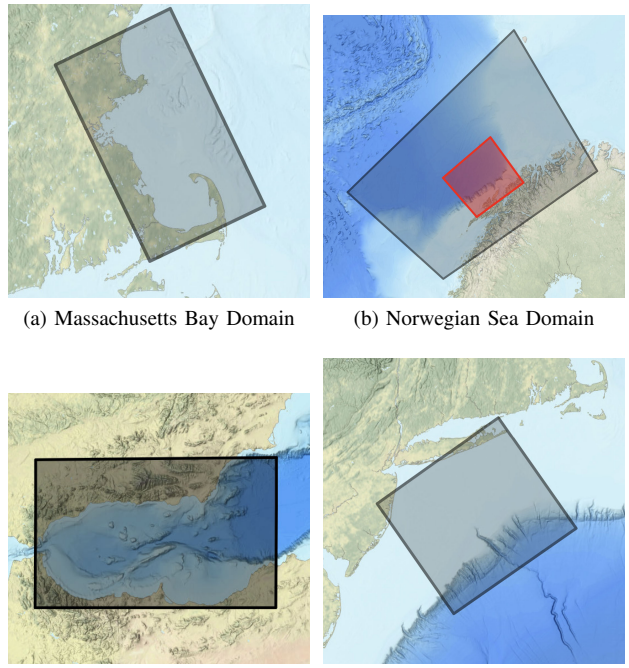

(a) Massachusetts Bay Domain (b) Norwegian Sea Domain

(c) Western Mediterranean Domain (d) NY Bight Domain

Fig. 1: Modeling domains for the (a) Massachusetts Bay, (b) Norwegian Sea, (c) western Mediterranean Sea, and (d) New York Bight regions. The red regions indicate nested sub-domains of interest. The topography and bathymetric data shown were obtained from the GEBCO_2022 grid [68].

A. Massachusetts Bay Forecasting Experiment 2019

The MSEAS-PE model was set up off the northeast US coast using the 3-arcsecond USGS Gulf of Maine digital elevation model [69]. The modeling domain is shown in figure 1a. It uses 333 m horizontal resolution with 100 optimized vertical levels, tidal forcing from TPXO8-Atlas [70, 71] (adapted to the high-resolution bathymetry and coastlines [51]), and atmospheric forcing from the 3 km North American Mesoscale Forecast System (NAM) from NCEP [72]. The subtidal initial and boundary conditions were downscaled from $1/12°$ analyses from the HYbrid Coordinate Ocean Model (HYCOM) [73, 74], using our optimization for higher resolution coastlines and bathymetry [40], and using corrections based on National Marine Fisheries Service (NMFS) data from August 28, 2019 [75]. The MSEAS-PE was run from August 11 to September 13, 2019. These ocean simulations were validated against independent data (e.g., NOAA NDBC buoy data [76]), and demonstrated skill by producing similar diurnal cycle excursions in SST, as well as good temporal alignment of SST trends and events. For a further discussion of the hindcast skill, as well as an analysis of the effects of several wind events, tides, internal tides, and solitary waves off Stellwagen Bank seen in these simulations, we refer to [49].

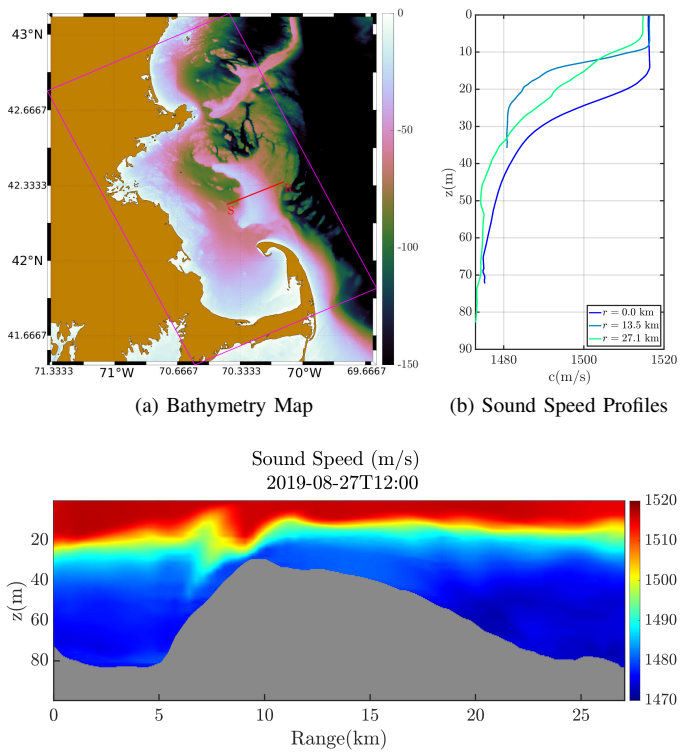

(a) Bathymetry Map

(b) Sound Speed Profiles

(c) Sound Speed Forecast

Fig. 2: Massachusetts Bay 2019. (a) Bathymetry map and section location. (b) MSEAS-PE forecast sound speed profiles for August 27, 2019, 12:00 UTC at the starting, middle, and final range of the section. (c) MSEAS-PE forecast sound speed field in the section.

The characteristics of Stellwagen Bank internal waves have been thoroughly analyzed [53, 77–79]. However, their effects on acoustic propagation have not been studied comprehensively. Here, we used our coupled MSEAS-ParEq solver to predict the acoustic TL from a harmonic source in a 2D section across the Bank. The section location and bathymetry map are shown in figure 2a. Figure 2b shows the MSEAS-PE hindcast sound speed profiles for August 27, 2019, 12:00 UTC, at the starting ($r = 0$), middle ($r = 13.55$ km), and final ($r = 27.1$ km) ranges within the section. Figure 2c shows the full sound speed field. The bottom in this section has a steep bank slope between the 5 and 10 km ranges, with bathymetry changing from 80 m to approximately 30 m. The effects of the internal tides are clearly visible in the sound speed field where strong vertical advection and mixing occurs near the seamount. We place a harmonic sound source at the initial range and vary its depth to study the effect of such shallow features on acoustic propagation. In figure 3, we show two TL predictions obtained using MSEAS-ParEq with the source located at $z_s = 5$ m and $z_s = 30$ m, respectively. The sediment properties in the Stellwagen Bank National Marine Sanctuary have been previously studied and our area of interest is predominantly characterized as sand [80], so the sound speed, density, and attenuation of sand sediments were used for the bottom. Comparing the two TL fields, the effects of the nonlinear internal tides are clearly visible. For the shallow source ($z_s = 5$ m), most of the acoustic energy is diverged by the solitary wave into the bottom where it is significantly attenuated. However, the deeper source ($z_s = 30$ m) has much less transmission loss in the region past the seamount.

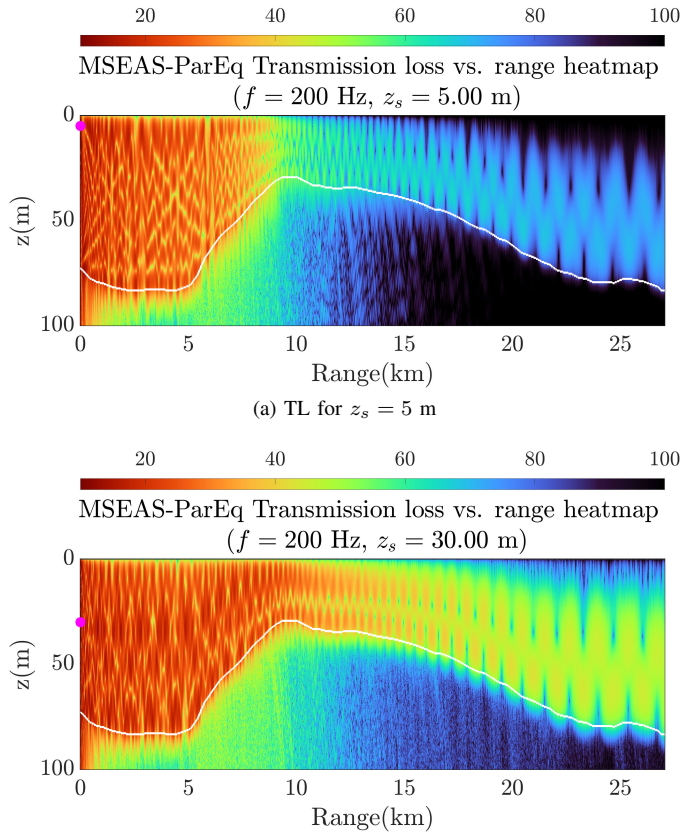

(a) TL for $z_s = 5$ m

(b) TL for $z_s = 30$ m

Fig. 3: Massachusetts Bay 2019. TL predictions from MSEAS-ParEq for a harmonic source with frequency $f = 200$ Hz located at (a) $z_s = 5$ m and (b) $z_s = 30$ m, respectively. Cylindrical spreading was removed from the TL calculation.

B. Norwegian Sea (2017)

For the Norwegian Sea (off Lofoten and the continental shelf), the MSEAS-PE modeling system was set up in an implicit two-way nested configuration using the Shuttle Radar Topography Mission (SRTM) 15-arcsecond global map [81–83]. Thus, two domains were utilized: (i) a $1/225°$-resolution domain in the vicinity of the acoustic sources and receivers, which was two-way nested inside (ii) a large, regional domain at $1/75°$ resolution (used for some standalone simulations); see figure 1b. Each domain had 100 optimized vertical levels. The tidal forcing again came from TPXO8 and the hourly atmospheric forcing from the NCEP 0.2° Climate Forecast System (CFS) model [84]. Our MSEAS-PE simulations were downscaled from $1/12°$ HYCOM, with optimized velocities. They assimilated fifteen quality-controlled Argo temperature and salinity profiles [85], covering the period January 3–11, 2017. Qualitative skill for our hindcast was seen in the SSH gradients (compared with AVISO satellite SSH [86]) and

large-scale features along the continental shelf. In addition, comparisons with Argo profiles showed that our corrections to temperature and salinity were generally maintained.

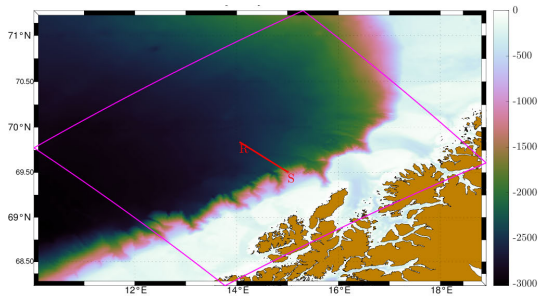

(a) Bathymetry Map

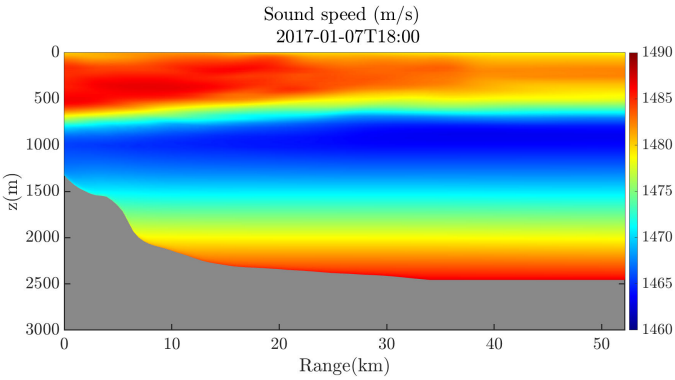

(b) Sound Speed Hindcast

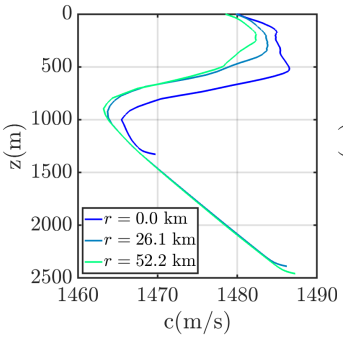

(c) Jan. 7th, 18:00 UTC

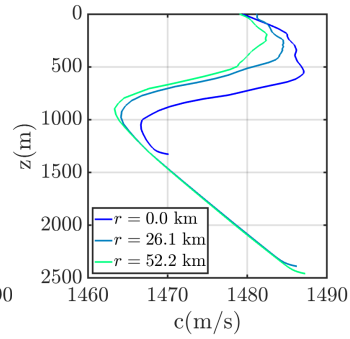

(d) Jan. 8th, 12:00 UTC

Fig. 4: Norwegian Sea 2017. (a) Bathymetry map along with the section location. (b) MSEAS-PE hindcast sound speed field in the section for January 7th, 2017, 18:00 UTC. (c) ad (d) Hindcast sound speed profiles at the starting, middle, and final ranges on January 7, 18:00 UTC, and January 8, 12:00 UTC, respectively.

Coupled with the MSEAS-PE, the MSEAS-ParEq predicted the TL fields in several 2D sections. We were specifically interested in acoustic propagation across and along the Norwegian Continental Shelf. One particular 2D section of interest is shown in figure 4a. The MSEAS-PE ocean hindcasts showed that the Norwegian Atlantic Current brings warmer waters from the south into the acoustic study region. Meanders in this current draw fresher water off the shelf into the acoustic domain. This is clearly visible in the sound speed hindcast shown in figure 4b. The surface duct above 300 m depth and a deep sound channel at around 900 m are also visible. To study the effects of ocean variability, we considered multiple time windows within the January 3–11 period. In figures 4c and 4d, we show the sound speed profiles at the beginning ($r = 0$), middle ($r = 26.1$ km), and final ($r = 52.2$ km) ranges for January 7, 18:00 UTC, and January 8, 12:00 UTC, respectively. Comparing the two figures, the effect of the Norwegian Atlantic Current and the meanders can be seen where both combine to introduce along-section variability in the upper 500 m of the sound speed. Additionally, internal tides and waves (ITs/IWs) radiating off the shelf introduce vertical excursions of the sound speed minimum of 30 m to 50 m as they pass through the section.

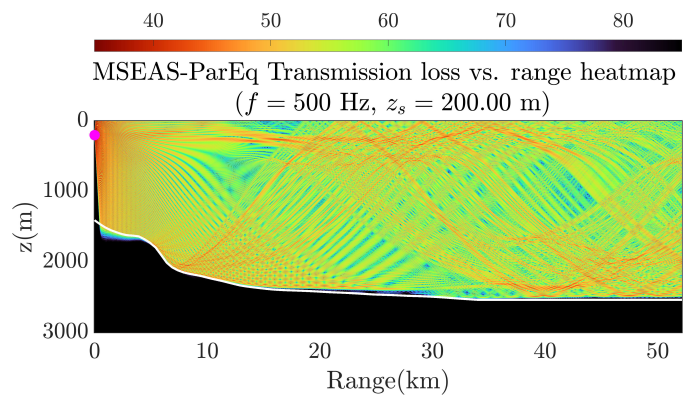

(a) TL at Jan. 7th, 18:00 UTC

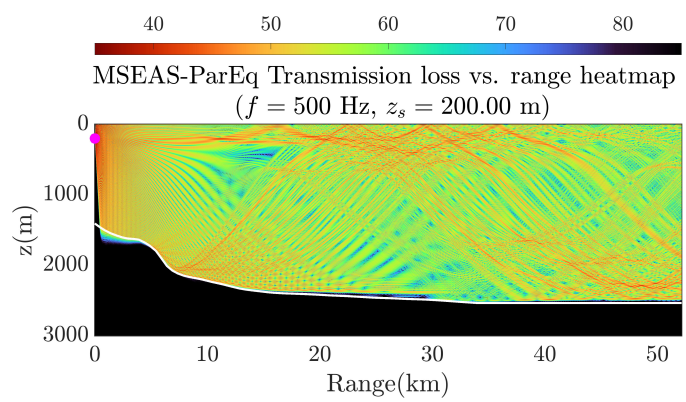

(b) TL at Jan. 8th, 12:00 UTC

Fig. 5: Norwegian Sea 2017. TL predictions from MSEAS-ParEq for a harmonic source with frequency $f = 500$ Hz and source depth $z_s = 200$ m using the sound speed hindcast for (a) January 7, 2017, 18:00 UTC, and (b) January 8, 2017, 12:00 UTC, respectively. Cylindrical spreading was removed from the TL calculation.

The TL fields predicted by MSEAS-ParEq for a harmonic point source of frequency $f = 500$ Hz located at $z_s = 200$ m in depth for both times are shown in figure 5. Additionally, figure 6 shows the differences between the two TL fields. The top panel shows the TL at a receiver located at $z_r = 200$ m. The heatmap in the panel below shows the difference field $TL_{\text{Jan7}} - TL_{\text{Jan8}}$. These results highlight significant differences in the acoustic propagation within the surface duct between the ranges of 15 and 20 km, in addition to within the deep sound

channel around the depth of 1000 km, especially between the ranges of 30 and 50 km.

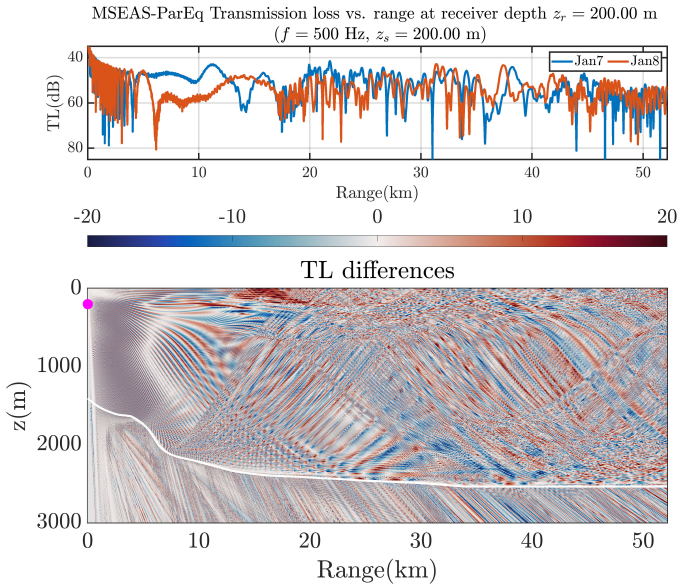

Fig. 6: Norwegian Sea 2017. Differences in TL predictions for January 7, 2017, 18:00 UTC, and January 8, 2017, 12:00 UTC, using the corresponding sound speed hindcasts. The top panel shows both TL curves at a receiver located at $z_r = 200$ m. The panel below shows the difference field $TL_{\text{Jan7}} - TL_{\text{Jan8}}$.

Finally, to validate our results for the Norwegian sea, we compared our MSEAS-ParEq TL predictions to RAM TL predictions. We found excellent agreement as highlighted by the RAM TL prediction shown in figure 7 using the MSEAS-PE sound speed hindcast for January 8, 2017, 12:00 UTC.

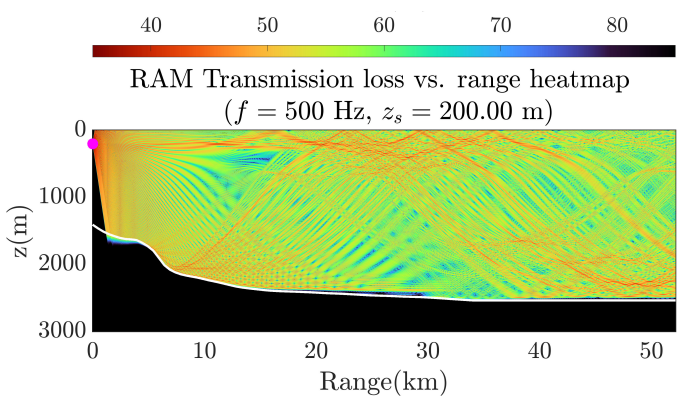

Fig. 7: Norwegian Sea 2017. TL predictions as in figure 5b, but using RAM. Results show excellent agreement with the MSEAS-ParEq TL predictions.

C. Western Mediterranean Sea (2016)

For the western Mediterranean Sea region, the MSEAS-PE model was set up using SRTM15 bathymetry. The resulting domain, shown in figure 1c, had a horizontal resolution of $1/200°$ (557 m) and was vertically discretized using 70 optimized vertical levels. These simulations were forced with tides from TPXO8, and with hourly atmospheric forcing from $0.2°$ NCEP CFS. As with the other cases, the system was initialized from downscaled $1/12°$ HYCOM, with velocities optimized. As in the Norwegian Sea, very limited data of opportunity were used to correct the HYCOM fields. These model runs cover the period November 16–30, 2016.

In these simulations, waters from the Atlantic flowing eastward in the upper layers meet the Mediterranean water flowing west around 2.25°W. This creates an instance of the Almeria–Oran front which is visible in the upper 75 m of the sound speed section around the 50 km range. Additionally, ITs and IWs radiating off the bathymetry create vertical excursions from 25 m to about 50 m in the sound speed along the section, as shown in the sound speed profiles in figure 8c. Skill was demonstrated by comparison to independent Argo profiles: agreement within 1°C and 0.25 psu was seen, the largest errors being in the thermo-/halocline. After the passing of a gale from November 16–21, the hindcasts beat persistence, with improvements in RMSE ranging between 20% and 40%.

Using these inputs from the MSEAS-PE high-resolution ocean simulations, we used our MSEAS-ParEq solver to predict shallow-to-deep and deep-to-shallow TL fields. To determine appropriate seafloor acoustic parameters, a survey of geoacoustic studies [87, 88] was completed. The TL fields we predicted as a function of range for November 23, 2016, at 12:00 UTC across a 2D section in the domain. The location of the section overlaid on bathymetry is shown in figure 8a along with the sound speed field hindcast from MSEAS-PE in figure 8b. Figure 8c shows sound speed profiles at the starting ($r = 0$), middle ($r = 57.4$ km), and final ($r = 114.8$ km) ranges. Below the surface layers, the sound speed field does not exhibit strong range variations. The surface channel above approximately 40 m and a deeper channel around 200 m are observed at all ranges. TL predictions in the shallow-to-deep (source located on the shallow plateau, left in figure 8b) and deep-to-shallow (source located on the deep plateau, right in figure 8b) sections are shown in figures 9a-9b, respectively, for a source located at 200 ft (approximately 92 m) in depth with a 1000 Hz frequency. The TL field maps show how the sound is distributed throughout the water column. In addition to the surface channels, convergence zones cause the sound to be re-focused at regular spatial intervals near the surface at ranges of approximately 20, 40, 60, 80, and 100 km. Bottom interactions have stronger effects in the case of the shallow-to-deep propagation case. We validated these TL predictions using RAM [89]. Figure 10 shows the RAM TL prediction for shallow-to-deep case. Comparisons with the MSEAS-ParEq prediction in figure 9a show excellent agreement.

D. New York Bight (2009)

Finally, our coupled system was used during a hindcast experiment for the New York Bight as part of an effort to characterize surface duct oceanographic variability and uncertainty. The modeling domain is shown in figure 1d. The ocean grid had a horizontal resolution of 1 km, with 100 vertical terrain-following levels. The period of interest spanned June 26 to

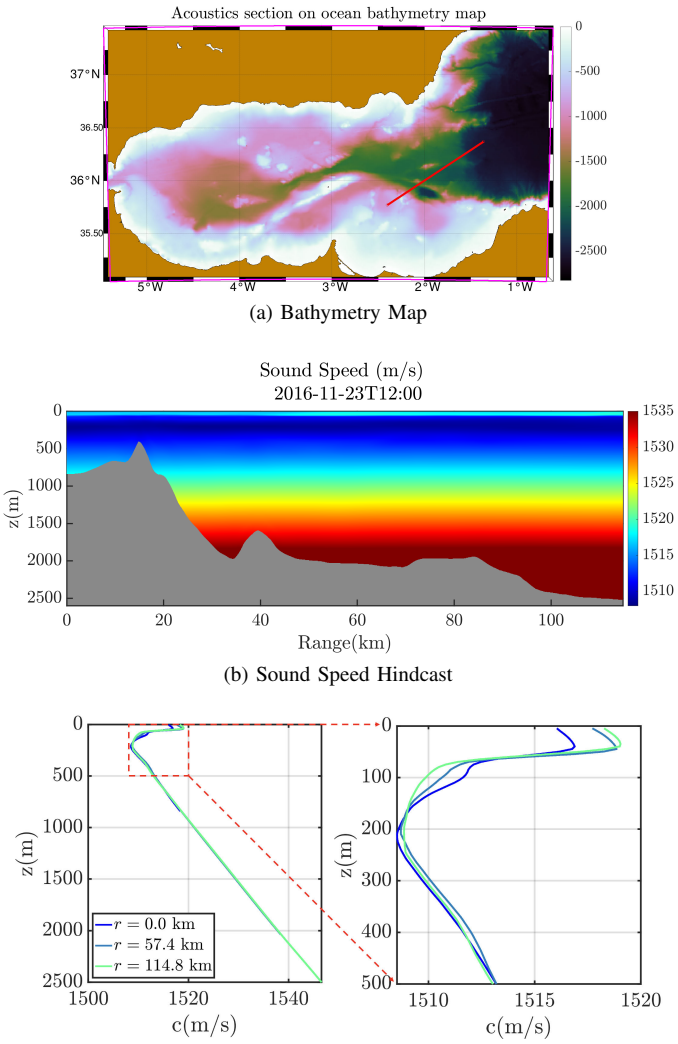

(a) Bathymetry Map

(b) Sound Speed Hindcast

(c) Sound Speed Profiles

Fig. 8: Western Mediterranean Sea 2016. (a) Bathymetry map along with the section location. (b) MSEAS-PE hindcast sound speed field in the section for November 23, 2016, 12:00 UTC. (c) MSEAS-PE hindcast sound speed profiles at the starting, middle, and final ranges starting from the shallow plateau, with a zoom in the upper 500 m depth.

July 5, 2009. The hindcasts were initialized from HYCOM and downscaled to higher resolution. They were forced by atmospheric flux fields from 32 km NCEP NAM, as well as by tidal forcing from TPXO8, but adapted to the high-resolution bathymetry and coastlines. We leveraged limited independent synoptic data of opportunity along with our feature modeling capabilities [19, 90] to correct the downscaled HYCOM fields; these corrections to the ICs reduced the ocean RMSE and bias by factors of 3 and 50, respectively. A more detailed discussion of the flow features, tidal effects, and hindcast skill of these ocean simulations can be found in [30].

MSEAS-ParEq was used to predict the TL and integrated TL fields across 2D sections in the New York Bight domain, using the MSEAS-PE ocean fields as inputs. The TL fields were computed for multiple source-receiver configurations at different times and frequencies. In figure 11, we only show

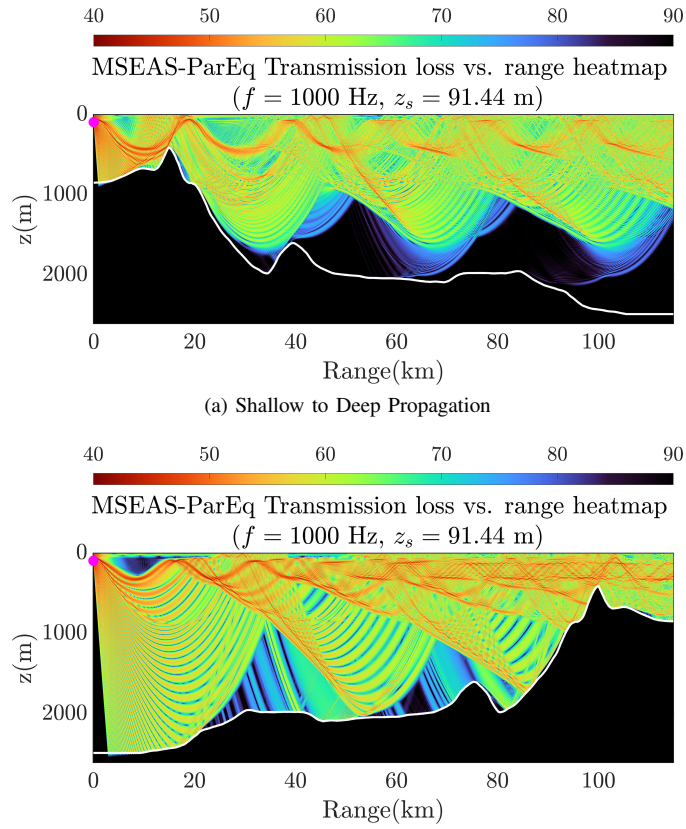

(a) Shallow to Deep Propagation

(b) Deep to Shallow Propagation

Fig. 9: Western Mediterranean Sea 2016. TL predictions from MSEAS-ParEq for a harmonic source with frequency $f = 1000$ Hz and source depth $z_s = 200$ ft ($\approx$ 92 m) using the sound speed hindcast for November 23, 2016, 12:00 UTC. (a) Propagation for the shallow-to-deep case, (b) Propagation for the deep-to-shallow case. Cylindrical spreading was removed from the TL calculation.

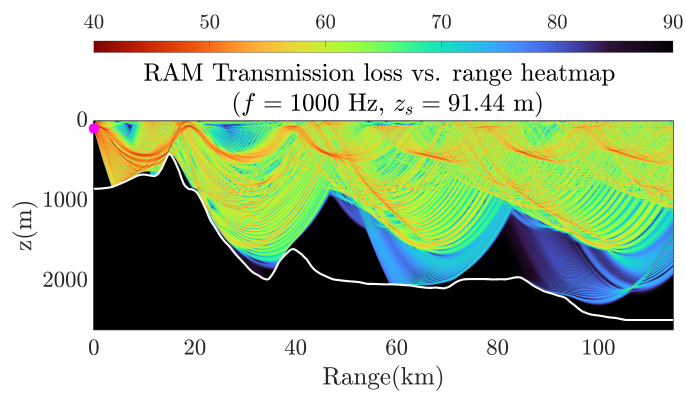

Fig. 10: Western Mediterranean Sea 2016. TL predictions as in figure 9a, but using RAM. Results show excellent agreement with the MSEAS-ParEq TL predictions.

the results obtained for one representative section with a time-harmonic source of frequency 950 Hz located at 65 ft ($\approx$ 20 m) depth. Figure 11a shows the section location and the bottom topography. The MSEAS-PE ocean modeling system provided a hindcast of the ocean physics fields including sound speed, as shown in the section of interest in figure 11b.

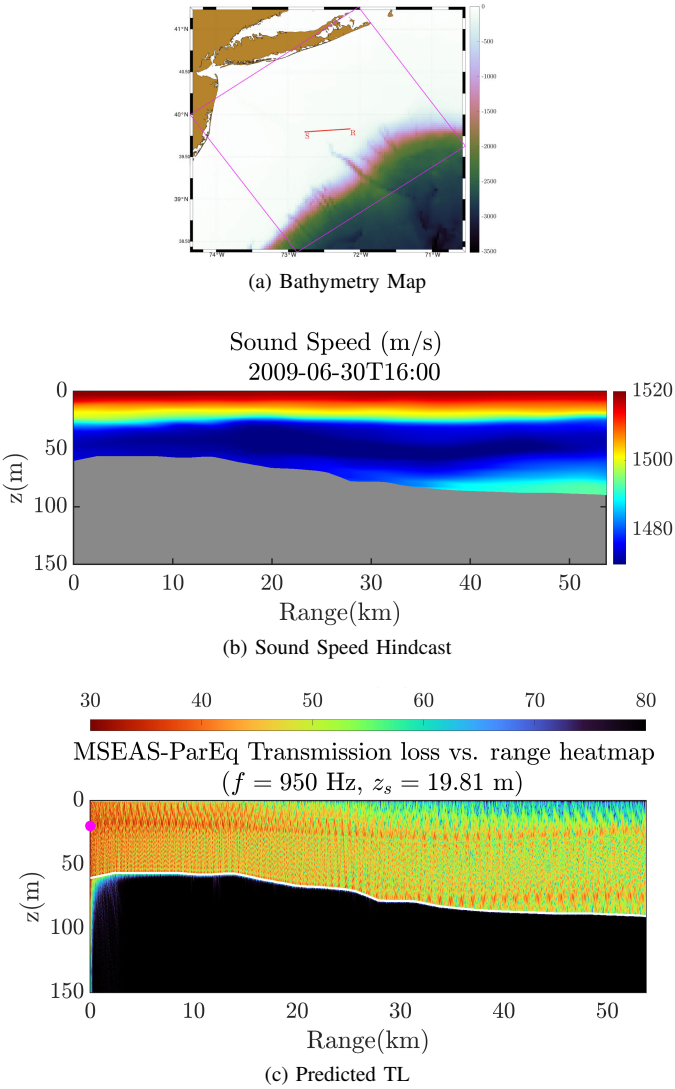

(a) Bathymetry Map

(b) Sound Speed Hindcast

(c) Predicted TL

Fig. 11: New York Bight 2009. (a) Bathymetry map along with the section location. (b) MSEAS-PE hindcast sound speed field in the section for June 30, 2009, 16:00 UTC. (c) MSEAS-ParEq predicted TL from a harmonic source of frequency $f = 950$ Hz located at $z_s = 65$ ft (≈ 19.81 m). Cylindrical spreading was removed from the TL calculation.

For the MSEAS-ParEq simulations in this shallow-water case, the seabed properties are of critical importance for accurate acoustic modeling [4, 91]. The New York Bight domain coincides with the Shallow Water '06 area, a region whose seabed has been studied and examined in multiple sea experiments [92]. Prior studies highlighted the relatively high prevalence of clay in the upper layers of the seabed [93, 94]. A fluid bottom with clay properties was thus used for sound speed, density, and attenuation in the MSEAS-ParEq. The resulting TL, using the sound speed inputs from the MSEAS-PE in figure 11b, are exemplified in figure 11c. To validate the MSEAS-ParEq predictions, we compared the integrated TL at sample receiver locations to data collected during a sea test that occurred off the New Jersey continental shelf at the end of June 2009. As discussed in [30], our ocean and acoustic simulations showed significant skill.

IV. Conclusion

We developed and evaluated a multi-resolution coupled ocean-acoustic modeling system for realistic deterministic ocean and acoustic regional predictions around the globe. This integration of our MIT MSEAS Primitive Equation (PE) ocean modeling system with the MSEAS acoustic parabolic equation (ParEq) model provides a powerful framework for predicting acoustic pressure and transmission loss fields, accounting for local bottom topography, seabed properties, and dynamic sound speed and density fields. Results were demonstrated in four ocean regions for low to mid-frequency propagation in both shallow and deep water environments. In each use case, we highlighted the impact of the ocean structure and its variability on the acoustic propagation characteristics in terms of surface and bottom reflections, surface ducts within the mixed layer, downward refractions, ducting within the deep sound channel, and shadow zone effects.

The tight coupling of multi-resolution ocean and acoustic modeling systems offers promising prospects for refining our understanding and forecasting of oceanic processes and their effects on acoustic propagation. Future steps towards deploying end-to-end coupled ocean-acoustic stochastic modeling systems can build on the efficient Dynamically Orthogonal Equations framework and its application to the ocean primitive equations [95] and acoustic parabolic equations [34, 36, 37]. After quantifying the ocean and acoustic uncertainties, and predicting the resulting stochastic fields [31, 96], joint dynamic inversion of the ocean physics and acoustic fields and model formulations, learning from the sparse acoustic and oceanographic data. This can be done by extending our nonlinear Bayesian data assimilation and machine learning framework [97–104] to ocean-acoustic inference tasks. All these goals are critical steps toward end-to-end systems for new ocean management and advanced operations.

Acknowledgments

We thank all members of the MSEAS group, past and present. We are grateful to the Office of Naval Research (ONR) for support under grant N00014-19-1-2664 (Task Force Ocean: DEEP-AI) to the Massachusetts Institute of Technology. We thank Phil Abbot, Ching-Sang Chiu, Emanuel Coelho, Tim Duda, Kevin Heaney, Paul Hursky, Andone Lavery, Nick Makris, and Henrik Schmidt for acoustics discussions over the years. Finally, we thank the HYCOM team for their ocean fields, as well as NCEP for their atmospheric forecasts.

References

[1] L. M. Brekhovskikh and Y. Lysanov, *Fundamentals of Ocean Acoustics*. Springer, 1982.

[2] H. Medwin and C. S. Clay, "Chapter 1 - the realm of acoustical oceanography; theory and applications of ocean acoustics," in *Fundamentals of Acoustical Oceanography*, ser. Applications of Modern Acoustics, H. Medwin and C. S. Clay, Eds. San Diego: Academic Press, 1998, pp. 1 – VI.

[3] F. B. Jensen, W. A. Kuperman, M. B. Porter, and H. Schmidt, *Computational ocean acoustics*. Springer Science & Business Media, 2011.

[4] P. C. Etter, *Underwater acoustic modeling and simulation*. CRC press, 2018.

[5] A. R. Robinson and P. F. J. Lermusiaux, "Prediction systems with data assimilation for coupled ocean science and ocean acoustics," in *Proceedings of the Sixth International Conference on Theoretical and Computational Acoustics*, A. Tolstoy et al, Ed. World Scientific Publishing, 2004, pp. 325–342, refereed invited Keynote Manuscript.

[6] P. F. J. Lermusiaux, J. Xu, C.-F. Chen, S. Jan, L. Chiu, and Y.-J. Yang, "Coupled ocean–acoustic prediction of transmission loss in a continental shelfbreak region: Predictive skill, uncertainty quantification, and dynamical sensitivities," *IEEE Journal of Oceanic Engineering*, vol. 35, no. 4, pp. 895–916, Oct. 2010.

[7] P. F. J. Lermusiaux and C.-S. Chiu, "Four-dimensional data assimilation for coupled physical-acoustical fields," in *Acoustic Variability, 2002*, N. G. Pace and F. B. Jensen, Eds. Saclantcen: Kluwer Academic Press, 2002, pp. 417–424.

[8] F.-P. A. Lam, P. J. Haley, Jr., J. Janmaat, P. F. J. Lermusiaux, W. G. Leslie, M. W. Schouten, L. A. te Raa, and M. Rixen, "At-sea real-time coupled four-dimensional oceanographic and acoustic forecasts during Battlespace Preparation 2007," *Journal of Marine Systems*, vol. 78, no. Supplement, pp. S306–S320, Nov. 2009.

[9] T. F. Duda, Y.-T. Lin, A. E. Newhall, K. R. Helfrich, J. F. Lynch, W. G. Zhang, P. F. J. Lermusiaux, and J. Wilkin, "Multiscale multiphysics data-informed modeling for three-dimensional ocean acoustic simulation and prediction," *Journal of the Acoustical Society of America*, vol. 146, no. 3, pp. 1996–2015, Sep. 2019.

[10] P. Abbot and I. Dyer, *Sonar Performance Predictions Incorporating Environmental Variability*. Dordrecht: Springer Netherlands, 2002, pp. 611–618.

[11] A. R. Robinson, S. M. Glenn, W. L. Siegmann, D. Lee, and G. Botseas, *Environmental Sensitivity Studies with an Interfaced Ocean - Acoustics System*. Dordrecht: Springer Netherlands, 1991, pp. 545–559.

[12] B. M. Howe, J. Miksis-Olds, E. Rehm, H. Sagen, P. F. Worcester, and G. Haralabus, "Observing the oceans acoustically," *Frontiers in Marine Science*, vol. 6, p. 426, 2019.

[13] W. Munk and C. Wunsch, "Ocean acoustic tomography: A scheme for large scale monitoring," *Deep Sea Research Part A. Oceanographic Research Papers*, vol. 26, no. 2, pp. 123–161, 1979.

[14] J. L. Spiesberger and K. Metzger, "Basin-scale ocean monitoring with acoustic thermometers," *Oceanography*, vol. 5, no. 2, pp. 92–98, 1992.

[15] B. D. Dushaw, "Ocean acoustic tomography in the north atlantic," *Journal of Atmospheric and Oceanic Technology*, vol. 36, no. 2, pp. 183 – 202, 2019.

[16] A. R. Robinson, P. Abbot, P. F. J. Lermusiaux, and L. Dillman, "Transfer of uncertainties through physical-acoustical-sonar end-to-end systems: A conceptual basis," in *Acoustic Variability, 2002*, N. G. Pace and F. B. Jensen, Eds. SACLANTCEN, Kluwer Academic Press, 2002, pp. 603–610.

[17] R. L. Culver and H. J. Camin, "Sonar signal processing using probabilistic signal and ocean environmental models," *The Journal of the Acoustical Society of America*, vol. 124, no. 6, pp. 3619–3631, 12 2008.

[18] A. Storto, G. D. Magistris, S. Falchetti, and P. Oddo, "A neural network–based observation operator for coupled ocean–acoustic variational data assimilation," *Monthly Weather Review*, vol. 149, no. 6, pp. 1967 – 1985, 2021.

[19] P. F. J. Lermusiaux, C. Mirabito, P. J. Haley, Jr., W. H. Ali, A. Gupta, S. Jana, E. Dorfman, A. Laferriere, A. Kofford, G. Shepard, M. Goldsmith, K. Heaney, E. Coelho, J. Boyle, J. Murray, L. Freitag, and A. Morozov, "Real-time probabilistic coupled ocean physics-acoustics forecasting and data assimilation for underwater GPS," in *OCEANS 2020 IEEE/MTS*. IEEE, Oct. 2020, pp. 1–9.

[20] N. Pinardi, L. Cavaleri, G. Coppini, P. D. Mey, C. Fratianni, J. Huthnance, P. F. J. Lermusiaux, A. Navarra, R. Preller, and S. Tibaldi, "From weather to ocean predictions: an historical viewpoint," *Journal of Marine Research*, vol. 75, no. 3, pp. 103–159, May 2017, special issue: The Science of Ocean Prediction, vol. 17 of The Sea.

[21] A. Tolstoy, "3-D propagation issues and models," *Journal of Computational Acoustics*, vol. 04, no. 03, pp. 243–271, 1996.

[22] A. R. Robinson, "Dynamical forecasting of mesoscale fronts and eddies for acoustical applications," *The Journal of the Acoustical Society of America*, vol. 82, no. S1, pp. S43–S43, 1987.

[23] G. Botseas, D. Lee, and W. Siegmann, "IFD: Interfaced with Harvard Open Ocean Model Forecasts," *Naval Underwater Systems Center Technical Report*, vol. 8367, 1989.

[24] D. Lee, G. Botseas, W. Siegmann, and A. Robinson, "Numerical computations of acoustic propagation through three-dimensional ocean eddies," in *Proceedings of the 12th IMACS World Congress*, 1989, pp. 19–22.

[25] C. Chiu and L. Ehret, "Computation of sound propagation in a three-dimensionally varying ocean: A coupled normal mode approach," *Computational Acoustics*, vol. 1, pp. 187–202, 1990.

[26] W. Siegmann, D. Lee, and G. Botseas, "Finite difference computations of three-dimensional sound propagation," *Computational Acoustics: Wave Propagation*, pp. 91–109, 1988.

[27] D. Wang, P. F. J. Lermusiaux, P. J. Haley, Jr., D. Eickstedt, W. G. Leslie, and H. Schmidt, "Acoustically focused adaptive sampling and on-board routing for marine rapid environmental assessment," *Journal of Marine Systems*, vol. 78, no. Supplement, pp. S393–S407, Nov. 2009.

[28] F. Gerdes and S. Finette, "A stochastic response surface formulation for the description of acoustic propagation through an uncertain internal wave field," *The Journal of the Acoustical Society of America*, vol. 132, no. 4, pp. 2251–2264, 10 2012.

[29] A. Storto, S. Falchetti, P. Oddo, Y.-M. Jiang, and A. Tesei, "Assessing the impact of different ocean analysis schemes on oceanic and underwater acoustic predictions," *JGR: Oceans*, vol. 125, no. 7, p. e2019JC015636, 2020.

[30] P. F. J. Lermusiaux, P. J. Haley, Jr., C. Mirabito, W. H. Ali, M. Bhabra, P. Abbot, C.-S. Chiu, and C. Emerson, "Multi-resolution probabilistic ocean physics-acoustic modeling: Validation in the New Jersey continental shelf," in *OCEANS 2020 IEEE/MTS*. IEEE, Oct. 2020, pp. 1–9.

[31] P. F. J. Lermusiaux, "Uncertainty estimation and prediction for interdisciplinary ocean dynamics," *Journal of Computational Physics*, vol. 217, no. 1, pp. 176–199, 2006.

[32] P. Hursky, M. B. Porter, B. D. Cornuelle, W. S. Hodgkiss, and W. A. Kuperman, "Adjoint modeling for acoustic inversion," *The Journal of the Acoustical Society of America*, vol. 115, no. 2, pp. 607–619, 01 2004.

[33] H. Ngodock, M. Carrier, J. Fabre, R. Zingarelli, and I. Souopgui, "A variational data assimilation system for the range dependent acoustic model using the representer method: Theoretical derivations," *The Journal of the Acoustical Society of America*, vol. 142, no. 1, pp. 186–194, 07 2017.

[34] W. H. Ali, "Dynamically orthogonal equations for stochastic underwater sound propagation," Master's thesis, Massachusetts Institute of Technology, Computation for Design and Optimization Program, Cambridge, Massachusetts, Sep. 2019.

[35] W. H. Ali, M. S. Bhabra, P. F. J. Lermusiaux, A. March, J. R. Edwards, K. Rimpau, and P. Ryu, "Stochastic oceanographic-

acoustic prediction and Bayesian inversion for wide area ocean floor mapping," in *OCEANS 2019 MTS/IEEE SEATTLE*. Seattle: IEEE, Oct. 2019, pp. 1–10.

[36] W. H. Ali and P. F. J. Lermusiaux, "Dynamically Orthogonal Narrow-Angle Parabolic Equations for Stochastic Underwater Sound Propagation," *Journal of the Acoustical Society of America*, 2023, in press.

[37] ——, "Dynamically Orthogonal Wide-Angle Parabolic Equations for Stochastic Underwater Sound Propagation," *Journal of the Acoustical Society of America*, 2023, in preparation.

[38] ——, "Joint Ocean-Acoustic Inversion using Gaussian Mixture Models and the Dynamically Orthogonal Parabolic Equations," 2023, in preparation.

[39] P. J. Haley, Jr. and P. F. J. Lermusiaux, "Multiscale two-way embedding schemes for free-surface primitive equations in the "Multidisciplinary Simulation, Estimation and Assimilation System"," *Ocean Dynamics*, vol. 60, no. 6, pp. 1497–1537, Dec. 2010.

[40] P. J. Haley, Jr., A. Agarwal, and P. F. J. Lermusiaux, "Optimizing velocities and transports for complex coastal regions and archipelagos," *Ocean Modeling*, vol. 89, pp. 1–28, 2015.

[41] F. D. Tappert, "The parabolic approximation method," in *Wave Propagation and Underwater Acoustics*, ser. Lecture Notes in Physics, Berlin Springer Verlag, J. B. Keller and J. S. Papadakis, Eds., vol. 70, 1977, p. 224.

[42] W. G. Leslie, A. R. Robinson, P. J. Haley, Jr, O. Logutov, P. A. Moreno, P. F. J. Lermusiaux, and E. Coelho, "Verification and training of real-time forecasting of multi-scale ocean dynamics for maritime rapid environmental assessment," *Journal of Marine Systems*, vol. 69, no. 1, pp. 3–16, 2008.

[43] P. J. Haley, Jr., P. F. J. Lermusiaux, A. R. Robinson, W. G. Leslie, O. Logoutov, G. Cossarini, X. S. Liang, P. Moreno, S. R. Ramp, J. D. Doyle, J. Bellingham, F. Chavez, and S. Johnston, "Forecasting and reanalysis in the Monterey Bay/California Current region for the Autonomous Ocean Sampling Network-II experiment," *Deep Sea Research Part II: Topical Studies in Oceanography*, vol. 56, no. 3–5, pp. 127–148, Feb. 2009.

[44] P. F. J. Lermusiaux, D. N. Subramani, J. Lin, C. S. Kulkarni, A. Gupta, A. Dutt, T. Lolla, P. J. Haley, Jr., W. H. Ali, C. Mirabito, and S. Jana, "A future for intelligent autonomous ocean observing systems," *Journal of Marine Research*, vol. 75, no. 6, pp. 765–813, Nov. 2017, the Sea. Volume 17, The Science of Ocean Prediction, Part 2.

[45] D. N. Subramani, P. J. Haley, Jr., and P. F. J. Lermusiaux, "Energy-optimal path planning in the coastal ocean," *Journal of Geophysical Research: Oceans*, vol. 122, pp. 3981–4003, 2017.

[46] C. S. Kulkarni, P. J. Haley, Jr., P. F. J. Lermusiaux, A. Dutt, A. Gupta, C. Mirabito, D. N. Subramani, S. Jana, W. H. Ali, T. Peacock, C. M. Royo, A. Rzeznik, and R. Supekar, "Real-time sediment plume modeling in the Southern California Bight," in *OCEANS Conference 2018*. Charleston, SC: IEEE, Oct. 2018.

[47] A. Gupta, P. J. Haley, D. N. Subramani, and P. F. J. Lermusiaux, "Fish modeling and Bayesian learning for the Lakshadweep Islands," in *OCEANS 2019 MTS/IEEE SEATTLE*. Seattle: IEEE, Oct. 2019, pp. 1–10.

[48] P. F. J. Lermusiaux, M. Doshi, C. S. Kulkarni, A. Gupta, P. J. Haley, Jr., C. Mirabito, F. Trotta, S. J. Levang, G. R. Flierl, J. Marshall, T. Peacock, and C. Noble, "Plastic pollution in the coastal oceans: Characterization and modeling," in *OCEANS 2019 MTS/IEEE SEATTLE*. Seattle: IEEE, Oct. 2019, pp. 1–10.

[49] P. J. Haley, Jr., A. Gupta, C. Mirabito, and P. F. J. Lermusiaux, "Towards Bayesian ocean physical-biogeochemical-acidification prediction and learning systems for Massachusetts Bay," in *OCEANS 2020 IEEE/MTS*. IEEE, Oct. 2020, pp. 1–9.

[50] P. J. Haley, Jr., C. Mirabito, M. Doshi, and P. F. J. Lermusiaux, "Ensemble forecasting for the Gulf of Mexico Loop Current region," in *OCEANS 2023 IEEE/MTS Gulf Coast*. Biloxi, MS: IEEE, Sep. 2023, in press.

[51] O. G. Logutov and P. F. J. Lermusiaux, "Inverse barotropic tidal estimation for regional ocean applications," *Ocean Modelling*, vol. 25, no. 1–2, pp. 17–34, 2008.

[52] A. Agarwal and P. F. J. Lermusiaux, "Statistical field estimation for complex coastal regions and archipelagos," *Ocean Modelling*, vol. 40, no. 2, pp. 164–189, 2011.

[53] P. F. J. Lermusiaux, "Evolving the subspace of the three-dimensional multiscale ocean variability: Massachusetts Bay," *Journal of Marine Systems*, vol. 29, no. 1, pp. 385–422, 2001.

[54] ——, "Estimation and study of mesoscale variability in the Strait of Sicily," *Dynamics of Atmospheres and Oceans*, vol. 29, no. 2, pp. 255–303, 1999.

[55] P. F. J. Lermusiaux, "Adaptive modeling, adaptive data assimilation and adaptive sampling," *Physica D: Nonlinear Phenomena*, vol. 230, no. 1, pp. 172–196, 2007.

[56] P. F. J. Lermusiaux, P. J. Haley, Jr, and N. K. Yilmaz, "Environmental prediction, path planning and adaptive sampling: sensing and modeling for efficient ocean monitoring, management and pollution control," *Sea Technology*, vol. 48, no. 9, pp. 35–38, 2007.

[57] Ş. T. Beşiktepe, P. F. J. Lermusiaux, and A. R. Robinson, "Coupled physical and biogeochemical data-driven simulations of Massachusetts Bay in late summer: Real-time and post-cruise data assimilation," *Journal of Marine Systems*, vol. 40–41, pp. 171–212, 2003.

[58] G. Cossarini, P. F. J. Lermusiaux, and C. Solidoro, "Lagoon of Venice ecosystem: Seasonal dynamics and environmental guidance with uncertainty analyses and error subspace data assimilation," *Journal of Geophysical Research: Oceans*, vol. 114, no. C6, Jun. 2009.

[59] P. F. J. Lermusiaux, C.-S. Chiu, and A. R. Robinson, "Modeling uncertainties in the prediction of the acoustic wavefield in a shelfbreak environment," in *Proceedings of the 5th International Conference on Theoretical and Computational Acoustics*, E.-C. Shang, Q. Li, and T. F. Gao, Eds. World Scientific Publishing Co., May 21-25 2002, pp. 191–200, refereed invited manuscript.

[60] J. Xu, P. F. J. Lermusiaux, P. J. Haley Jr., W. G. Leslie, and O. G. Logutov, "Spatial and Temporal Variations in Acoustic propagation during the PLUSNet-07 Exercise in Dabob Bay," in *Proceedings of Meetings on Acoustics (POMA)*, vol. 4. Acoustical Society of America 155th Meeting, 2008, p. 11.

[61] T. F. Duda, Y.-T. Lin, W. Zhang, B. D. Cornuelle, and P. F. J. Lermusiaux, "Computational studies of three-dimensional ocean sound fields in areas of complex seafloor topography and active ocean dynamics," in *Proceedings of the 10th International Conference on Theoretical and Computational Acoustics*, Taipei, 2011.

[62] M. E. G. D. Colin, T. F. Duda, L. A. te Raa, T. van Zon, P. J. Haley, Jr., P. F. J. Lermusiaux, W. G. Leslie, C. Mirabito, F. P. A. Lam, A. E. Newhall, Y.-T. Lin, and J. F. Lynch, "Time-evolving acoustic propagation modeling in a complex ocean environment," in *OCEANS - Bergen, 2013 MTS/IEEE*, 2013, pp. 1–9.

[63] F. Sturm and J. A. Fawcett, "On the use of higher-order azimuthal schemes in 3-d pe modeling," *JASA*, vol. 113, no. 6, pp. 3134–3145, 2003.

[64] J. F. Claerbout, *Fundamentals of geophysical data processing*. Citeseer, 1985.

[65] M. D. Collins, "A self-starter for the parabolic equation method," *The Journal of the Acoustical Society of America*, vol. 92, no. 4, pp. 2069–2074, 10 1992.

[66] ——, "The stabilized self-starter," *The Journal of the Acoustical Society of America*, vol. 106, no. 4, pp. 1724–1726, 10 1999.

[67] T. Ryu, W. H. Ali, P. J. Haley, Jr., C. Mirabito, A. Charous, and P. F. J. Lermusiaux, "Incremental low-rank dynamic mode decomposition model for efficient dynamic forecast dissemination and onboard forecasting," in *OCEANS 2022 IEEE/MTS*. Hampton Roads, VA: IEEE, Oct. 2022, pp. 1–8.

[68] GEBCO Compilation Group, "The GEBCO_2022 grid," 2022.

[69] E. R. Twomey and R. P. Signell, "Construction of a 3-arcsecond digital elevation model for the Gulf of Maine," U.S. Geological Survey, Open-File Report 2011–1127, 2013.

[70] G. D. Egbert and S. Y. Erofeeva, "Efficient inverse modeling of barotropic ocean tides," *Journal of Atmospheric and Oceanic Technology*, vol. 19, no. 2, pp. 183–204, 2002.

[71] ——, "OSU tidal inversion," 2013. [Online]. Available: http://volkov.oce.orst.edu/tides/tpxo8_atlas.html

[72] National Centers for Environmental Prediction (NCEP), "The North American Mesoscale forecast system (NAM)," Jul. 2023, Accessed 2023-07-20. [Online]. Available: https://www.ncei.noaa.gov/products/weather-climate-models/north-american-mesoscale

[73] J. A. Cummings and O. M. Smedstad, *Variational Data Assimilation for the Global Ocean*. Berlin, Heidelberg: Springer Berlin Heidelberg, 2013, pp. 303–343.

[74] The HYCOM Consortium, "HYbrid Coordinate Ocean Model (HYCOM)," Feb. 2023, accessed 2019-04-09. [Online]. Available: https://hycom.org

[75] National Marine Fisheries Service, Aug. 2019. [Online]. Available: https://www.nefsc.noaa.gov/HydroAtlas/

[76] National Data Buoy Center (NDBC), https://www.ndbc.noaa.gov/, Sep. 2019.

[77] D. Halpern, "Observations of short period internal waves in massachusetts bay." Ph.D. dissertation, Massachusetts Institute of Technology, 1969.

[78] ——, "Semidiurnal internal tides in massachusetts bay," *Journal of Geophysical Research (1896-1977)*, vol. 76, no. 27, pp. 6573–6584, 1971.

[79] T. K. Chereskin, "Generation of internal waves in massachusetts bay," *Journal of Geophysical Research: Oceans*, vol. 88, no. C4, pp. 2649–2661, 1983.

[80] U. F. Sheet, "Mapping the sea floor and biological habitats of the stellwagen bank national marine sanctuary region," 1998.

[81] C. J. Olson, J. J. Becker, and D. T. Sandwell, "A new global bathymetry map at 15 arcsecond resolution for resolving seafloor fabric: SRTM15_PLUS," in *AGU Fall Meeting*. San Francisco: American Geophysical Union, Dec. 2014, pp. OS34A–03.

[82] ——, "SRTM15_PLUS: Data fusion of Shuttle Radar Topography Mission (SRTM) land topography with measured and estimated seafloor topography," Dataset, May 2016, NCEI Accession 0150537.

[83] B. Tozer, D. T. Sandwell, W. H. F. Smith, C. Olson, J. R. Beale, and P. Wessel, "Global bathymetry and topography at 15 arc sec: SRTM15+," *Earth and Space Science*, vol. 6, no. 10, pp. 1847–1864, Oct. 2019.

[84] National Centers for Environmental Prediction (NCEP), "Climate Forecast System (CFS)," https://www.ncei.noaa.gov/products/weather-climate-models/climate-forecast-system, Jul. 2023.

[85] Argo, "Argo float data and metadata from Global Data Assembly Centre (Argo GDAC)," 2000.

[86] E.U. Copernicus Marine Service Information (CMEMS). Marine Data Store (MDS), "Global ocean along track sea surface heights reprocessed," Jul. 2023.

[87] M. J. Null, P. J. Bucca, B. R. Gomes, N. OCEANOGRAPHIC, and A. R. L. S. S. C. MS, "Environmental assessment for selected regions in the mediterranean sea," Tech. Rep., 1992.

[88] P. Bárcenas-Gascón, F. J. Lobo, J. Macías, L. M. Fernández-Salas, and V. Díaz-del Río-Español, "Spatial variability of surficial sediments on the northern shelf of the alboran sea: the effects of hydrodynamic forcing and supply of sediment by rivers," *Centro Oceanográfico de Cádiz*, 2011.

[89] M. D. Collins, "User's guide for RAM versions 1.0 and 1.0 p," *Naval Research Lab, Washington, DC*, vol. 20375, p. 14, 1995.

[90] P. F. J. Lermusiaux, "Data assimilation via Error Subspace Statistical Estimation, part II: Mid-Atlantic Bight shelfbreak front simulations, and ESSE validation," *Monthly Weather Review*, vol. 127, no. 7, pp. 1408–1432, Jul. 1999.

[91] E. L. Hamilton, "Geoacoustic modeling of the sea floor," *The Journal of the Acoustical Society of America*, vol. 68, no. 5, pp. 1313–1340, 1980.

[92] D. Tang, J. N. Moum, J. F. Lynch, P. Abbot, R. Chapman, P. H. Dahl, T. F. Duda, G. Gawarkiewicz, S. Glenn, J. A. Goff *et al.*, "Shallow water'06: A joint acoustic propagation/nonlinear internal wave physics experiment," *Oceanography*, vol. 20, no. 4, pp. 156–167, 2007.

[93] M. S. Ballard, K. M. Becker, and J. A. Goff, "Geoacoustic inversion for the new jersey shelf: 3-d sediment model," *IEEE Journal of Oceanic Engineering*, vol. 35, no. 1, pp. 28–42, 2010.

[94] J. A. Goff and UT Inst. for Geophysics, "Stratigraphic and geoacoustic characterization of the outer new jersey shelf," Technical Report, DTIC Document, Tech. Rep., 2008.

[95] D. Subramani and P. F. J. Lermusiaux, "Probabilistic ocean predictions with dynamically-orthogonal primitive equations," 2023, in preparation.

[96] P. F. J. Lermusiaux, C.-S. Chiu, G. G. Gawarkiewicz, P. Abbot, A. R. Robinson, R. N. Miller, P. J. Haley, Jr, W. G. Leslie, S. J. Majumdar, A. Pang, and F. Lekien, "Quantifying uncertainties in ocean predictions," *Oceanography*, vol. 19, no. 1, pp. 92–105, 2006.

[97] T. Sondergaard and P. F. J. Lermusiaux, "Data assimilation with Gaussian Mixture Models using the Dynamically Orthogonal field equations. Part I: Theory and scheme." *Monthly Weather Review*, vol. 141, no. 6, pp. 1737–1760, 2013.

[98] ——, "Data assimilation with Gaussian Mixture Models using the Dynamically Orthogonal field equations. Part II: Applications." *Monthly Weather Review*, vol. 141, no. 6, pp. 1761–1785, 2013.

[99] T. Lolla and P. F. J. Lermusiaux, "A Gaussian mixture model smoother for continuous nonlinear stochastic dynamical systems: Theory and scheme," *Monthly Weather Review*, vol. 145, pp. 2743–2761, Jul. 2017.

[100] ——, "A Gaussian mixture model smoother for continuous nonlinear stochastic dynamical systems: Applications," *Monthly Weather Review*, vol. 145, pp. 2763–2790, Jul. 2017.

[101] P. Lu and P. F. J. Lermusiaux, "Bayesian learning of stochastic dynamical models," *Physica D: Nonlinear Phenomena*, vol. 427, p. 133003, Dec. 2021.

[102] A. Gupta and P. F. J. Lermusiaux, "Bayesian learning of coupled biogeochemical-physical models," *Progress in Oceanography*, vol. 216, p. 103050, May 2023.

[103] ——, "Neural closure models for dynamical systems," *Proceedings of The Royal Society A*, vol. 477, no. 2252, pp. 1–29, Aug. 2021.

[104] ——, "Generalized neural closure models with interpretability," *Scientific Reports*, 2023, in press. [Online]. Available: https://doi.org/10.1038/s41598-023-35319-w